Thermal stability and high-temperature shape memory characteristics of Ti–20Zr–10Ta alloy*

Zheng Xiao-Hang(郑晓航), Sui Jie-He(隋解和), Zhang Xin(张 欣), Yang Zhe-Yi(杨哲一), and Cai Wei(蔡 伟)†

National key Laboratory Precision Hot Processing of Metals, School of Materials Science and Engineering, Harbin Institute of Technology, Harbin 150001, *China*

(Received 20 June 2013; revised manuscript received 6 August 2013; published 19 November 2013)

The microstructure, martensite transformation behavior, thermal stability and shape memory behavior of Ti–20Zr–10Ta high temperature shape memory alloy were investigated. The Ti–20Zr–10Ta alloy exhibited a reversible transformation with the high martensite transformation temperature of 500 °C and good thermal stability. The alloy displayed the elongation of 15% and a maximum recovery stain of 5.5% with 8% pre-strain.

Keywords: Ti–Zr–Ta alloy, martensite transformation, high temperature shape memory effect, thermal stability

PACS: 81.30.Kf, 61.66.Dk **DOI:** 10.1088/1674-1056/23/1/018101

1. Introduction

A few high temperature shape memory alloys (HTSMAs) have been studied in recent years, such as Ti–Ni–X (X = Hf, Zr, Pt) alloys, Ni–Mn–X (X = Ga, In)-based and Ni-free Ti-based (Ti–Ta, Ti–Nb, Ti–Mo) alloys.[1–7] However, those HTSMAs mentioned above exhibit their best shape memory properties with a martensite transformation start temperature (Ms) of less than 400 °C.[8] In order to extend their applications in an engine's systems, the HTSMAs with a Ms higher than 400 °C must be explored. A few systems of HTSMAs have been reported that have stable Ms over 400 °C, such as Ti–X (X = Pd, Au, Zr) and Ru–X (X = Nb, Ta) alloys.[9–12] The Ti–Pd and Ti–Au alloys have the complete shape memory recovery of 3% with a Ms about 500 °C.[10] The Ru–Ta and Ru–Nb alloys possess a very high Ms over 900 °C. However, the very high cost of the Ti–X (X = Pd, Au) and Ru–X (X = Nb, Ta) alloys is an important issue for practical application.[13,14] Li Yan *et al.* reported that the Ti–Zr alloys exhibit a shape memory effect with the Ms temperature over 400 °C.[15,16] Furthermore, the cost of Ti–Zr alloys is much less than that of Ti–Pd and Ti–Au alloys; Ti–Zr alloys display a fracture strain of 8% and maximum recovery strain of less than 3% with the 5% pre-strain. The Ti–Zr brainy alloy shows $\alpha\prime$ martensite with a hexagonal structure, which causes a higher Young's modulus and lower shape memory effect than that of α'' martensite with an orthorhombic structure. In order to improve the high- temperature shape memory effect, 10-at% Nb has been added into the Ti–Zr alloy. The Ti–20Zr–10Nb alloy has orthorhombic α'' martensite, which exhibits an Ap of 565°C and a maximum recovery strain of 5% with 8% pre-strain.[16] However, the ω phase precipitation occurrs in Ti–20Zr–10Nb alloy, leading to the instability. Therefore, it is necessary to find another alloying element to increase the tensile ductility and shape memory properties of the Ti–Zr alloys without any ω phase precipitation. It is generally accepted that Ta is a better β-phase stabilizer element than Nb element.[17] Therefore, an appropriate amount of Ta addition as a substitute of Zr in the Ti–Zr alloy should be able to change the structure to orthorhombic and maintain a high Ms temperature as well. It has been reported that the structure is related to the valence electrons number per atom (e/a). The critical composition of Ta for an α'/α'' transition in Ti–Ta brainy alloy is 8.7 at% with the corresponding e/a of 4.09;[18] the e/a has been increased from 4 to 4.1 with the addition of 10-at% Ta compared with the Ti–30Zr alloy, so the Ti–20Zr–10Ta may exhibit an orthorhombic structure. Therefore, the influence of Ta on the microstructure, thermal stability, mechanical behavior and shape memory effect of the Ti–Zr alloy are investigated in this article.

2. Experiment

The Ti–20Zr–10Ta alloy was prepared on a non-consumable arc-melting furnace under an Ar atmosphere using a water-cooled copper crucible. The arc-melting was repeated eight times to ensure the uniformity of composition. After melting, the ingots were homogenized at 850 °C for 6 h in vacuum-sealed quartz tubes, then quenched in iced water. The specimens were cut into the desired shapes for various characterizations by a spark-erosion cutting machine. The phase structure was identified by X-ray diffraction (XRD) on a Riguku-D/max-rB X-ray diffractometer with Cu K_α radiation at room temperature. The microstructure of the alloy was investigated by a FEI TECNAI G2 20 STWIN 200 kV

*Project supported by the National Natural Science Foundation of China (Grant Nos. 51071059 and 51271065) and the National Basic Research Program of China (Grant No. 2012CB619400)

†Corresponding author. E-mail: weicai@hit.edu.cn

© 2014 Chinese Physical Society and IOP Publishing Ltd

transmission electron microscope equipped with a double-tilt cooling stage (TEM). The phase transformation temperature of the specimen was determined by differential thermal analysis (DTA) using Mettler–Toledo TGA1600. The DTA tests were carried out by heating the specimens to 700 °C and then cooled down to 300 °C with a heating/cooling rate of 20 K·min^{-1}. The tensile stress-strain tests were performed on the Instron-1186 machine with a strain rate of 10^{-4} s^{-1}.

3. Results and discussion

It has been reported that Ti–30Zr binary alloy is a hexagonal structure at room temperature. Figure 1 shows the XRD profile for the Ti–20Zr–10Ta solution treated specimen at room temperature. Diffraction peaks corresponding to the α'' phase with an orthorhombic structure can be observed in Ti–20Zr–10Ta alloy, indicating that the addition of 10-at% Ta changes the phase structure of the alloy, which is the target phase.

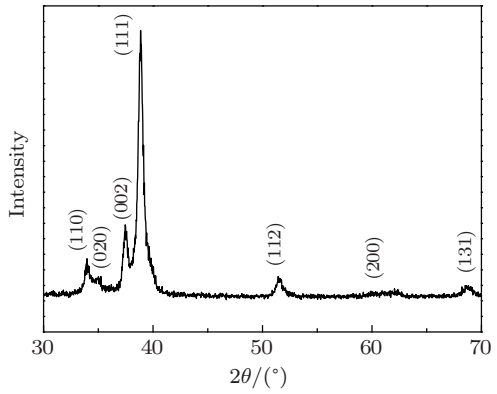


Fig. 1. XRD profile taken at room temperature for Ti–20Zr–10Ta solution treated specimen.

Figure 2 shows the TEM observation of the microstructure of Ti–20Zr–10Ta alloy. TEM bright field image of Ti–20Zr–10Ta reveals that there are fine internal twins in the α'' martensite plates. The internal twins extend from one side of the α'' plate to the other. The $[110]_{\alpha''}$ selected area electron diffraction (SAED) pattern and its index shown in Fig. 2 demonstrate that the internal twins are (11) Type I.

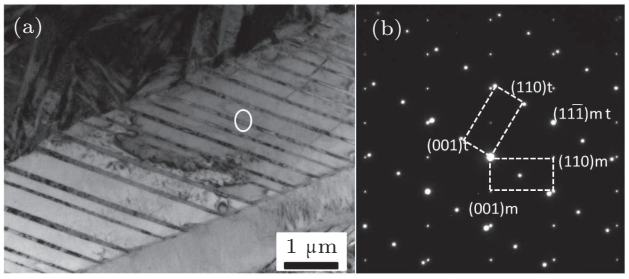


Fig. 2. (a) Bright field TEM image of solution treated Ti–20Zr–10Ta alloy and (b) corresponding diffraction patterns.

For the high temperature application, it is an important issue that the alloys have high and stable Ms after different thermal cycles. Figure 3(a) shows the DTA curves of Ti–20Zr–10Ta alloy as a function of the thermal cycle. The Ti–20Zr–10Ta alloy has a Ms temperature of 500 °C in the first thermal cycle. According to the previous report, the Ti–30Zr alloy has a Ms about 600 °C.[15] The decrease of the Ms could be ascribed to the Ta addition since Ta is a β-phase stabilizer element.[19] In order to investigate the thermal stability of Ti–20Zr–10Ta alloy, the specimen is thermally cycled between 300 °C and 700 °C up to 50 cycles. The peak temperatures of the matrensite transformation (Mp) and the matrensite reverse transformation (Ap) used to evaluate the cycling stability are shown in Fig. 3(b). In the first 30 cycles, the Mp temperature decreases slightly with the increase of the number of thermal cycles. After 30 thermal cycles, the Mp and Ap temperatures only drop 15 °C and 10 °C, respectively. The decrease of transformation temperature is due to the introduction of dislocation during the thermal cycles. It should be noted that there is no obvious change in the transformation temperature between 30 to 50 thermal cycles, indicating that Ti–20Zr–10Ta alloy has excellent thermal cycling stability.

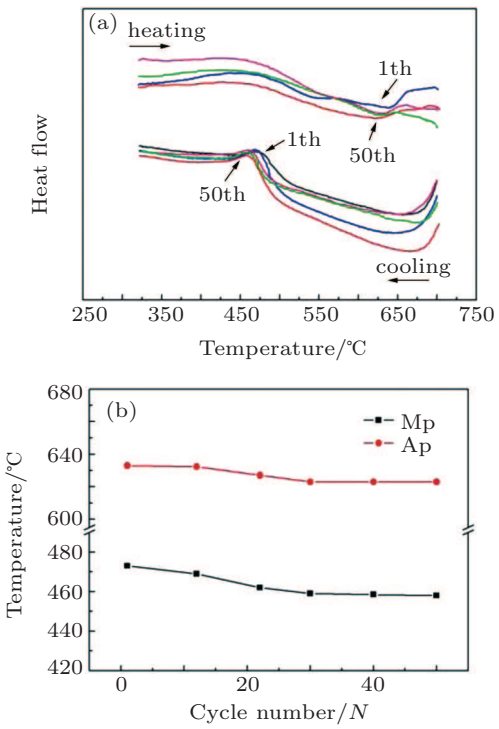


Fig. 3. (color online) DTA curves of Ti–20Zr–10Ta alloy with different thermal cycles (a) and the transformation temperature as a function of thermal cycling number for Ti–20Zr–10Ta alloy (b).

The $\overline{\text{Bo}}$–$\overline{\text{Md}}$ diagram is useful to design β-Ti-based alloys in the previous reports.[20,21] $\overline{\text{Bo}}$ and $\overline{\text{Md}}$ are the average bond orders between atoms and the average d-orbital energy level of elements in the alloy, respectively. The alloy position moves on the $\overline{\text{Bo}}$–$\overline{\text{Md}}$ diagram with the change of the alloy

composition. The $\overline{\text{Bo}}$ and $\overline{\text{Md}}$ can be given

$$\overline{\text{Bo}} = \sum_{i=1}^{n} x_i(\text{Bo})_i, \tag{1}$$

$$\overline{\text{Md}} = \sum_{i=1}^{n} x_i(\text{Md})_i, \tag{2}$$

where the x_i is the atomic percent of alloy element i.

The $\overline{\text{Bo}}$ and $\overline{\text{Md}}$ values of Ti–20Zr–10Ta alloy are 2.8846 and 2.5528, respectively. The position of Ti–20Zr–10Ta alloy in the $\overline{\text{Bo}}$–$\overline{\text{Md}}$ diagram is far from the $\beta/\beta+\omega$ boundary and below the boundary of Ms, leading to suppress the ω phase precipitation and maintain a high Ms temperature as well.

Figure 4(a) shows the stress-strain curves at room temperature for Ti–20Zr–10Ta alloy. It can be seen that Ti–20Zr–10Ta alloy exhibits a better ductility than that of Ti–Zr alloy. The Ti–20Zr–10Ta alloy displays a fracture strain of 15%, while the Ti–Zr binary alloys only have a fracture strain of less than 8%.[15] Figure 4(b) shows the loading and unloading curves of Ti–20Zr–10Ta alloy obtained from cyclic tensile testing; the dash line corresponds to the shape recovery strain after heating. It can be seen that both the recovered strain and the irrecoverable strain increase with the increase of the pre-strain. The maximum recovery strain is 5.5% with the 8% pre-strain. The Ti–30Zr alloy only has the maximum shape memory recovery strain less than 3% when it is deformed to a total strain of 5%.[15]

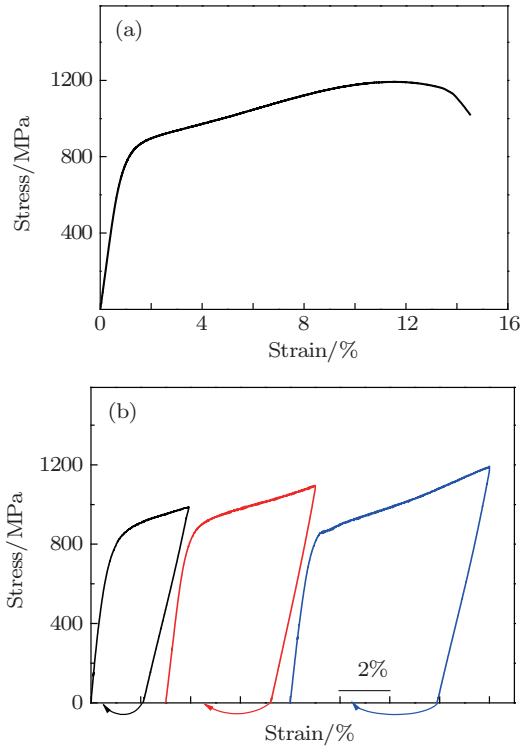


Fig. 4. (color online) (a) Tensile stress–strain curve of solution treated Ti–20Zr–10Ta alloy. (b) The cyclic loading and unloading curves of the Ti–20Zr–10Ta solution-treated specimen.

As mention above, with the addition of 10-at% Ta into the Ti–Zr alloy, the structure has been changed from hexagonal to orthorhombic and Young's modulus is decreased. Li Y *et al.* have reported that there is a relationship between the Young's modulus and the interatomic bonding force (f) in the Ti–Zr based alloy.[22] By combining Coulomb's law and d electrons alloy theory, the f can be estimated according to the equation[22]

$$f \propto \frac{\overline{Z_{\text{eff}}}\overline{\text{Bo}}}{\overline{\text{Md}}^2}, \tag{3}$$

where $\overline{Z_{\text{eff}}}$ is the compositional average value of effective nuclei charges (Z_{eff}). Considering the shielding effect by other electrons in each atom, the Z_{eff} can be calculated by Z–σ, where Z is the atomic number and σ is the Slater shielding constant. The $\overline{Z_{\text{eff}}}$ values of Ti–30Zr and Ti–20Zr–10Ta are 3.4 and 3.45, respectively. It has been reported that the same alloying element has different Bo values and the same Md value for different alloy structures.[22] According to the Bo and Md value list,[22] the $\overline{\text{Bo}}$ value significantly decreases from 3.5679 to 2.8846 with the addition of 10-at% Ta. The results show the bonding forces of Ti–30Zr and Ti–20Zr–10Ta are 1.593 and 1.527, respectively. The decrease of the interatomic bonding force leads to a decrease of the detwinning critical stress. Therefore, the martensite reorientation in Ti–20Zr–10Ta alloy may take place at lower stress without inducing plastic deformation, compared with that in Ti–30Zr alloy at higher stress. This may explain why the Ti–20Zr–10Ta alloy with an orthorhombic structure exhibits a better shape memory effect than that of the Ti–30Zr alloy with a hexagonal structure. In comparison with other HTSMAs in a similar transformation temperature range, the Ti–20Zr–10Ta alloy exhibits good ductility and thermal stability and equivalent shape memory properties with Ti–Au and Ti–Pd alloys. It is worth mentioning that the cost of the Ti—Zr–Ta alloy is much less than that of the Ti–Au and Ti–Pd alloys, which is also important for application. Therefore, the Ti–20Zr–10Ta alloy shows potential applications in high temperature shape memory actuators.

4. Conclusions

In conclusion, the influence of Ta on the microstructure, thermal stability and shape memory properties of Ti–30Zr HTSMA have been studied. The results demonstrate that the Ti–20Zr–10Ta alloy undergoes a reversible martensitic transformation with a high Ms of 500 °C. The Ti–20Zr–10Ta alloy also displays excellent thermal stability and good plasticity with a fracture strain of 15%. It has a maximum recovery strain of 5.5% with 8% pre-strain. Therefore, the Ti–20Zr–10Ta alloy is thought to be a good candidate in the field of actuators.

References

[1] Zhang X, Sui J H, Yu Z and Cai W 2011 *J. Alloys. Compd.* **509** 8032
[2] Kim H Y, Ikehara Y, Kim J I, Hosoda H and Miyazaki S 2006 *Acta Mater.* **54** 2419
[3] Miyazaki S, Kim H Y and Hosoda H 2006 *Mater. Sci. Eng. A* **438–440** 18
[4] Xu H, Ma Y and Jiang C 2003 *Appl. Phys. Lett.* **82** 3206
[5] Tobe H, Kim H Y, Inamura T, Hosoda H, Nam T H and Miyazaki S 2012 *J. Alloys. Compd.*
[6] Song R N, Zhu W, Liu E K, Li G J, Cai J F, Wang W H and Wu G H 2011 *Acta Phys. Sin.* **60** 77501 (in Chinese)
[7] Liu Z H, Li G T and Ma X Q 2012 *Acta Phys. Sin* **61** 108104 (in Chinese)
[8] Shen H H, Fu H, Guo Y J, Fu Y Q and Zu X T 2011 *Chin. Phys. B* **20** 46102
[9] Gao X, Cai W, Zheng Y F and Zhao L C 2006 *Mater. Sci. Eng. A* **438–440** 862
[10] Ma J, Karaman I and Noebe R D 2010 *Inter. Mater. Rev.* **55** 257
[11] Tian X H, Tan C L and Cai W 2012 *Chin. Phys. B* **21** 57105
[12] Tian X H, Tan C L and Cai W 2008 *Chin. Phys. Lett.* **25** 3372
[13] Wu C M and Wu S K 1987 *Metallography* **20** 359
[14] Kawakita M, Takahashi M, Takahashi S and Yamabe-Mitarai Y 2012 *Mater. Lett.* **89** 336
[15] Li Y, Cui Y, Zhang F and Xu H 2011 *Scripta Mater.* **64** 584
[16] Cui Y, Li Y, Luo K and Xu H 2010 *Mater. Sci. Eng. A* **527** 652
[17] Buenconsejo P J S, Kim H Y, Hosoda H and Miyazaki S 2009 *Acta Mater.* **57** 1068
[18] Boyer G W R R and Collings E W 1994 *Materials Properties Handbook Titanium Alloys* (USA: ASM International) p. 23
[19] Kim H Y, Hashimoto S, Kim J I, Inamura T, Hosoda H and Miyazaki S 2006 *Mater. Sci. Eng. A* **417** 120
[20] Abdel-Hady M, Fuwa H, Hinoshita K, Kimura H, Shinzato Y and Morinaga M 2007 *Scripta Mater.* **57** 1000
[21] Abdel-Hady M, Hinoshita K and Morinaga M 2006 *Scripta Mater.* **55** 477
[22] Li Y and Song X 2012 *Scripta Mater.* **67** 57